High-resolution measurements of Cl^{15+} line shifts in hot, solid-density plasmas

P. Beiersdorfer, G. V. Brown, A. McKelvey, and R. Shepherd
Physics Division, Lawrence Livermore National Laboratory, Livermore, California 94550, USA

D. J. Hoarty, C. R. D. Brown, M. P. Hill, L. M. R. Hobbs, S. F. James, J. Morton, and L. Wilson
Physics Department, AWE plc, Reading RG7 4PR, United Kingdom

(Received 6 August 2018; revised manuscript received 7 May 2019; published 17 July 2019)

The shifts of the $1s3p\,^1P_1 \rightarrow 1s^2\,^1S_0$ He-β transition of Cl^{15+} were measured in hot ($\geqslant$600 eV), dense (1–2 g/cm^3) plasmas generated by a (66–151)-J short-pulse laser beam at the Orion laser facility. The subpicosecond laser beam irradiated optically thin, KCl microdot targets buried in layers of plastic. The measured red shifts ranged from 4.8 ± 1.1 eV for unshocked to 5.9 ± 1.2 eV for shocked targets. These values are significantly smaller than recent predictions from a self-consistent-field ion-sphere model.

DOI: 10.1103/PhysRevA.100.012511

Atomic systems embedded in a plasma encounter effects that are absent for isolated ions in a vacuum. Bound electrons experience fields produced by the surrounding particles that perturb their energy levels, resulting in line broadening, continuum lowering, and line shifts. Because a true vacuum does not exist, one may argue that the energy levels of all atomic systems differ from their ideal values. Such differences, however, are too small to measure. Perturbations in the energy levels become more pronounced as the electron density increases. The manifestations of these perturbations are predicted to be ubiquitous in hot plasmas near solid densities, such as those achieved in inertial confinement fusion (ICF) and the interior of stars. The broadening of the $1s3p \rightarrow 1s^2$ resonance lines in highly charged ions was observed and employed early on to measure the density of laser-compressed ICF capsules [1]. This is understandable because Stark-induced line broadening is the easiest phenomenon to observe and can be measured at ICF-type high densities even with rather low-resolution spectrometers. By contrast, continuum lowering, or ionization potential depression [2], has only recently been studied in highly charged ions, yielding surprisingly controversial results [3,4]. Furthermore, the plasma-induced line shift is predicted to represent only a fraction of the linewidth [5] and is therefore considered the most difficult of the three external field induced effects to observe and quantify. Apart from requiring high-resolution, well calibrated spectrometers for plasma-induced line-shift measurements, the shifts can be masked by a variety of subtle source or instrumental effects, such as by the presence of dielectronic satellite lines [6] or by spatial shifts of the emitting plasma, e.g., caused by laser ablation, which translate into spectral shifts when using flat or cylindrically or conically bent crystals for energy dispersion of the spectral emission.

So far, line-shift measurements have concentrated on the $2p \rightarrow 1s$ Lyman-α or He-α lines [7–12]. These measurements employed elements with atomic charge no higher than $Z = 13$ (aluminum), as a lower nuclear charge enables a larger fractional perturbation of the energy levels by the plasma electrons. Moreover, no definitive measurements of the line shift of $3p \rightarrow 1s$ lines exist, although such β lines are preferred diagnostics of high-density plasmas because, unlike the α lines, they are only weakly affected by opacity effects, yet they are strongly affected by Stark broadening. Pioneering work by Saemann *et al.* on the Lyman-α or He-α lines included measurements of the He-β line of Al^{11+} [9], but that line was found to be dwarfed by satellite lines from Li-like ions and therefore did not yield a definitive measurement of the shift. An analysis of the $1s3p \rightarrow 1s^2$ He-β line in Ar^{16+} used in ICF as a density diagnostic indicated a redshift that increased with plasma density [13]. However, the shift was only on the order of the instrumental resolution and the accuracy was further affected by the calibration of the dispersion and line-shape fitting procedures. The first definitive measurement of a β line shift was obtained only recently for the Kβ line of neutral iron [14].

In the following, we present a definitive measurement of the shift of the $1s3p\,^1P_1 \rightarrow 1s^2\,^1S_0$ He-β transition of Cl^{15+} in solid-density plasmas. The measurements were carried out with a very-high-resolution spectrometer, which clearly showed the spectral line shape and did not limit the accuracy of our measurement. Moreover, the plasma temperature is sufficiently high to suppress satellite lines that might otherwise mask a shift of the line.

Measurements of field-induced line shifts have benefited greatly from advances in short-pulse laser technology, which allow the isochoric heating of a given target, i.e., before hydrodynamic expansion takes place, and a number of line-shift measurements have employed such lasers [9,10,12]. In the following, we use similar technology albeit at higher laser energies than employed before, which enables us to employ targets with tamper thicknesses greater than or equal to 10 μm in order to eliminate any ablation of the buried microdot material and to allow for shocking the target.

Our measurements were carried out at the Orion laser facility located at Aldermaston in the United Kingdom. The Orion laser comprises ten 500-J, 0.351-μm long-pulse beams

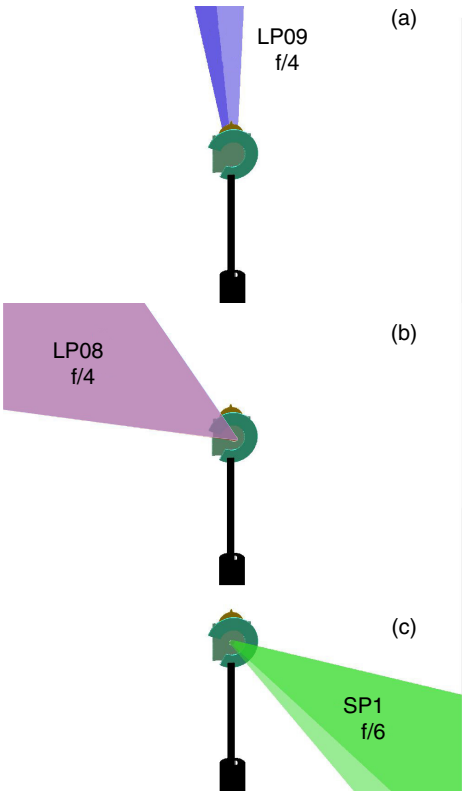

FIG. 1. View of the target holder and target as seen by the OHREX spectrometer. For comparison, the orientation of (a) long-pulse beam LP09, (b) long-pulse beam LP08, and (c) short-pulse beam SP1 are shown.

and two 500-J, 1.054-μm short-pulse beams [15]. One of the two short-pulse laser beams can be operated at 0.527 μm, and we employed this beam to carry out our experiments. Frequency doubling suppresses the prepulse inherent in conventional infrared laser systems and enables contrast ratios on the order of 10^{12} [16]. The high-contrast ratio enables efficient heating of solid targets [17–21]. In addition, we used two of the long-pulse beams to establish the spectral calibration of our spectra.

The measurements shown here were made with the Orion high-resolution x-ray spectrometer (dubbed OHREX), which was described earlier [22]. For the present measurements, the OHREX sightline views the target 15° off the target normal, as illustrated in Fig. 1.

OHREX is situated outside the 4-m-diam Orion vacuum chamber and employs two spherically bent crystals. The instrument's spherical dispersion geometry focuses x rays of a given energy onto the same spectral position even if they emanate from an extended plasma source as large as a tokamak plasma [23]. As a result, spatial shifts of the plasma do not translate into spectral shifts. This geometry thus eliminates a problem that has afflicted, for example, flat-crystal spectrometer geometries.

For the present measurements, both crystals are quartz $(11\bar{2}0)$ with a lattice spacing $2d = 4.912$ Å. Because OHREX is set to a nominal Bragg angle of $\theta = 51.3°$, both crystals record the chlorine He-β spectrum so that each laser shot gives us two spectra. The spatial focus was not optimized because the broadened spatial image enabled us to identify and eliminate potential hard-x-ray hits. By contrast, the instrument's spectral focus was estimated to exceed resolving powers in excess of 10 000, as described earlier [22,24,25].

Unlike its original version [22], the spectrometer setup used in our experiment was upgraded to utilize a charge-coupled device (CCD) camera instead of an image plate for recording the spectral data [26]. This was a necessary upgrade to ensure that reference-line fiducials from calibration shots could be used to establish a reliable energy scale for all other shots in the measurement sequence. Previously, a given line fell onto slightly different parts of the image plate each time the plate was exchanged between laser shots. The only shot-to-shot fiducials available were the start and end of the spectral region illuminated by the crystal. However, because of a low continuum emission and background, these were often not readily identifiable. As a result, the overall uncertainty with which the position of a given line could be determined from shot to shot with the image-plate detector was only about 5 eV, which was equal to or higher than the shifts reported in the present work. Indeed, our past measurements with the image plate setup did not show any line shifts larger than this uncertainty.

The fact that we employ a CCD camera means that the spectral emission is integrated over the entire plasma duration. However, as part of our diagnostics suite we have time-resolved, albeit lower-resolution, spectrometers that resolve the time history of the emission. These show that the emission lasts no more than about 20 ps, which is shorter than the time needed for buried target material to blow apart. Simulations show that the density of the buried target material stays constant within ±15% during this time. The calculated temperature evolves much faster, and its rise and decay are consistent with the emission history recorded by the time-resolved spectrometers.

In Fig. 2 we show traces of the Cl^{15+} He-β emission produced by one of the two quartz crystals in OHREX. These traces were obtained from targets irradiated with one of the long-pulse laser beams and are meant to establish the energy scale of the observed spectra.

Figure 2 depicts two spectra. The "smooth" spectrum from Orion shot 10144 was produced by firing a 177-J, 0.5-ns square pulse beam from beam line LP09 onto a 3-μm-thick parylene dichloride (PyD) foil. The laser spot diameter was about 300 μm. As a result, the emitted x-ray flux is strong, producing the high signal-to-noise ratio, smooth trace shown in Fig. 2. This trace allows us to identify not only the $1s3p\ ^1P_1 \rightarrow 1s^2\ ^1S_0$ He-β transition of Cl^{15+}, but also its inner shell and dielectronic satellite lines located on the low-energy side of the He-β line. These satellite lines are very weak and are indicative of a high electron temperature. A similar spectrum obtained with OHREX had been reported earlier [27], and we refer to this paper for a detailed discussion of the satellite lines.

The second spectrum shown in Fig. 2 was produced by firing a 235-J, 1-ns square pulse beam (LP08) onto a KCl microdot buried within a 3-μm-thick parylene N (PyN) foil on the front and a 4-μm-thick PyN foil on the back (Orion shot

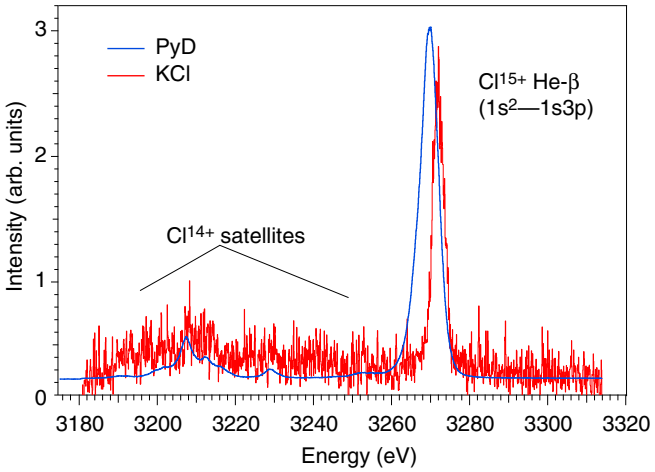

FIG. 2. Spectra of the Cl^{15+} He-β line and its Cl^{14+} satellite lines recorded with the OHREX spectrometer on Orion produced by long-pulse irradiation of a PyD foil (smooth, blue trace, Orion shot 10144) and of a tamped KCl microdot (noisy, red trace, Orion shot 10166). The latter trace was multiplied by 150 and shifted vertically to fit onto the same intensity scale. The peaks are Doppler shifted from one another due to the motion of the PyD plasma away from and of the KCl plasma toward the OHREX spectrometer's line of sight.

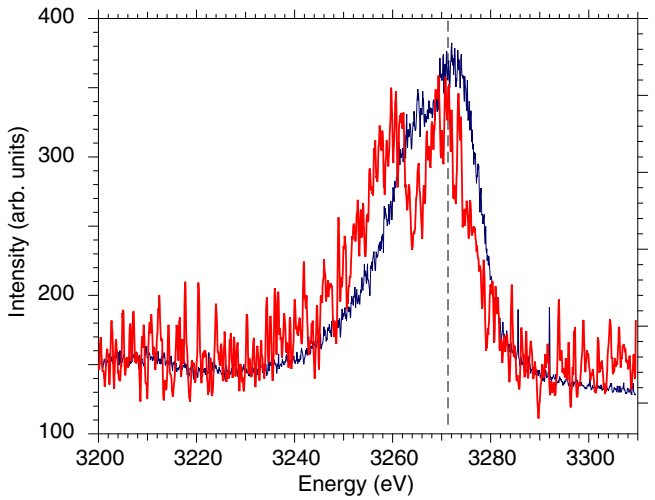

FIG. 3. Spectra showing the Cl^{15+} He-β line recorded with the OHREX spectrometer on the Orion laser and produced by short-pulse irradiation of a tamped PyD foil (smoother, blue trace, Orion shot 10140) and of a tamped KCl microdot (noisier, red trace, Orion shot 10142). The dashed vertical line indicates the location of the unshifted line. The vertical scale has been multiplied by 2×10^4 relative to the scale shown in Fig. 2.

10166). The dot is 0.38 μm thick and 50 μm in diameter. The resultant signal is about 150× weaker than the signal from the PyD target, and the spectrum exhibits much more noise than the other trace shown in Fig. 2. The reduced signal strength is roughly commensurate with the pulse length difference and the smaller number of chlorine ions in the KCl dot than in the irradiated spot of the PyD foil target.

The most striking difference when comparing the two spectral traces in Fig. 2 is that the peak of the He-β line in the KCl spectrum does not coincide with the peak in the PyD spectrum. The two He-β peaks are shifted from each other by 3.2 eV. This shift, however, is not surprising, because the plasma motion induced by long-pulse irradiation results in the ablation of hot plasma and thus in a Doppler shift. The hot plasma blows off preferentially normal to the irradiated surface so that an emitted line is blueshifted if the laser and the spectrometer view the same side and it is redshifted when the laser and spectrometer view opposite sides. The data in Fig. 2 were obtained by choosing long-pulse beams LP09 (opposite side) and LP08 (same side as the OHREX sightline) to irradiate our calibration targets, as illustrated in Fig. 1.

For subsequent analysis, we can assume that the unshifted peak should be located in the middle between the two peaks. We have checked this assumption in another calibration shot (10150), in which a 3-μm-thick vanadium foil was irradiated by a 155-J, 0.5-ns square pulse beam (LP09). The He-γ and He-δ lines of V^{21+} appear in our spectra in second order and thus provide another set of reference lines. Indeed, both lines were again shifted by 1.5 eV from their rest energy. The vanadium lines together with the Cl^{15+} He-β line and the strongest of the Cl^{14+} satellite peaks also provide us with a means to establish the energy dispersion of the two crystals in our spectrometer. We estimate that this procedure allowed us to establish the energy scale with an accuracy of 0.5 eV.

In Fig. 3 we show spectra obtained by irradiating the PyD and KCl targets with the 2ω short-pulse beam, labeled SP1 in Fig. 1. In particular, the PyD foil target was irradiated in Orion shot 10140 by a 0.65-ps, best focus, 66-J laser beam. The KCl microdot target was heated by a 0.58-ps, 50-μm focal spot, 151-J laser beam in Orion shot 10142. The 50-μm-diam, 0.38-μm-thick KCl dot was buried in a 10-μm (front) and 12-μm (back) PyN layer. A thicker overcoat was chosen in order to attempt shocking the target with a 118-J, 0.5-ns square pulse beam from LP09. In addition, we collected spectral data from two KCl microdot targets buried within a 3-μm (front) and 4-μm (back) parylene N (PyN) layer that were irradiated by a 124-J, 0.6-ps (Orion shot 10141) and a 84-J, 0.59-ps (Orion shot 10143) laser pulse. No attempt was made to compress these targets.

The spectra in Fig. 3 are plotted on the energy scale we derived as discussed above and the spectral location of the unshifted He-β line is indicated by a dashed vertical line. At first glance we note that both targets produce similar spectra, albeit the emission from the much thinner KCl target is again significantly weaker. Moreover, the observed He-β lines are much broader (FWHMs of 18 and 26 eV, respectively) than the observed widths in Fig. 2. The lines also exhibit an asymmetry indicative of Stark-induced broadening at high density, while the satellite lines from Li-like Cl^{14+} are similarly weak as seen before in Fig. 2. Finally and most importantly, we note that both He-β lines are clearly shifted to lower energies.

A closer look at the spectra in Fig. 3 shows that the line from the KCl target is somewhat broader than that from the PyD target. It also has a more pronounced central dip. When averaged over the data from both crystals in our spectrometer,

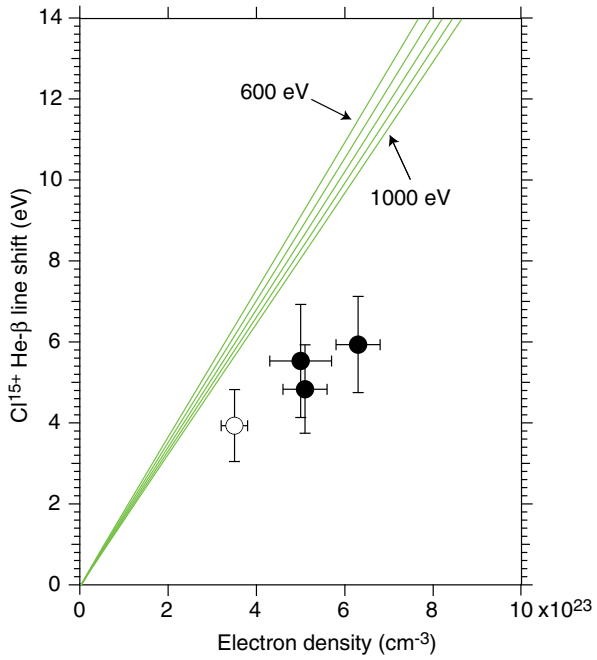

FIG. 4. Comparison of the measured and calculated redshift of the Cl^{15+} He-β line as a function of electron density. The experimental data are from Orion shots (left to right) 10140, 10141, 10143, and 10142. The calculated shift is based on the analytical expression given by [28] and is given for plasma temperatures (solid green lines) between 600 and 1000 eV in 100-eV increments. The temperatures associated with these measurements are estimated to lie between 600 and 650 eV.

we determine a shift $\Delta E_{\mathrm{PyD}} = 3.9 \pm 0.9$ eV for the PyD target shot, while we determine a shift $\Delta E_{\mathrm{KCl}} = 5.9 \pm 1.2$ eV for the KCl target shot. In both cases, the uncertainty in the measured shift results from locating the center of the line. The latter is potentially affected by the quality of the crystal bend, as was illustrated recently [26], where it was found that a given crystal focuses diffracted x rays better in some regions than in others, forming a netted pattern. We could check for this systematic effect by comparing the data from the two crystals in our setup and we therefore take the average of the two measurements.

In order to compare the measured shift to theory, we need to determine the density of the emitting plasma. For this, we can use the observed linewidth, which has a power-law dependence on density, as shown in [27]. From the 18.6 ± 0.5 eV width of the PyD He-β line we infer a density of $(3.5 \pm 0.3) \times 10^{23}$ cm^{-3}, while from the 26.2 ± 0.7 eV width of the KCl He-β line we infer a density of $(6.3 \pm 0.5) \times 10^{23}$ cm^{-3}. Both of these densities are near solid. For both cases we estimate an electron temperature of about 600–650 eV from the intensity ratio of the (weak) dielectronic satellite lines to the He-β line.

The experimental values of the line shifts for the four short-pulse irradiated targets are plotted in Fig. 4 against the respective densities inferred from the linewidths. Here we also show the predictions from the ion-sphere model proposed by Li and Rosmej (green traces) [28]. This model predicts a linear dependence on the electron density.

Li and Rosmej's line-shift model is fully analytical. It allows us to derive all relevant quantities for calculating the line shift from tabulated transition and ionization energies. For example, we get $Z_{\mathrm{eff}}(1s) = 16.915$ and $Z_{\mathrm{eff}}(3p) = 16.045$ for the effective charge seen by a $1s$ and a $3p$ electron, respectively. For the quantum average radii (in atomic units) we obtain $\langle r(1s)\rangle = 0.088\,68$ and $\langle r(3p)\rangle = 0.7790$, as well as $\langle r^2(1s)\rangle = 0.0105$ and $\langle r^2(3p)\rangle = 0.6992$. Because the model predicts that the line shift depends on the electron temperature, we have calculated shifts in the temperature range from 600 to 1000 eV in 100-eV increments, as indicated by the solid green lines in Fig. 4. This range of temperatures covers the range over which our time-integrated measurement potentially samples the emission from the plasma. Here we do not show lower temperatures because the He-β emission is strongly reduced at lower temperatures and thus is not expected to contribute significantly to the measured signal. Calculations show, for example, that the He-β emission is $10\times$ weaker at 400 eV than at 600 eV.

As seen from Fig. 4, our measured values are below the predicted values. In fact, the datum for the densest (shocked) plasma is a factor of 2 below the prediction. Interestingly, the experimental points from the recent measurements of the line shift of the He-α line of Al^{11+} [12] were all *higher* than predicted by Li and Rosmej's analytical line-shift model, albeit by smaller amounts.

In conclusion, we have definitively measured a spectral redshift of the $1s3p\,^1P_1 \rightarrow 1s^2\,^1S_0$ He-β transition of Cl^{15+} in hot, near-solid density plasmas. The high temperature ensures that satellite lines do not significantly contribute to the measured line shape or line shift; such contributions have adversely affected a clear measurement of the He-β line shift in the past [9].

Our measured values at the highest density disagrees with the analytical line-shift model developed by Li and Rosmej [28] by a factor of 2. Even though the measured shifts between 4 and 6 eV are lower than predicted by this model, they are at least four times larger than the lower limits placed on the shift by pioneering work [5], which estimated that the shifts are at least as large as 5% of the linewidth (greater than 1 eV in our case). Our measurements illustrate that the ultimate theoretical description of the line shift in the strong fields generated by a dense cloud of plasma electrons has not yet been attained.

It will be interesting to see whether the disagreement with theory expands to an even larger discrepancy at densities of 10 g/cm^3 and above. An order of magnitude higher density than we explore here is expected when multiple long-pulse beams are timed properly to shock the target while its is heated by the short-pulse beam. Such experiments will explore line shifts in regimes relevant to the densities found deep in the solar interior.

This work was performed under the auspices of the U.S. DOE by LLNL under Contract No. DE-AC52-07NA27344. P.B. wishes to thank C. Iglesias for helpful comments.

[1] B. A. Hammel, C. J. Keane, M. D. Cable, D. R. Kania, J. D. Kilkenny, R. W. Lee, and R. Pasha, Phys. Rev. Lett. **70**, 1263 (1993).

[2] D. R. Inglis and E. Teller, Astrophys. J. **90**, 439 (1939).

[3] O. Ciricosta, S. M. Vinko, H.-K. Chung, B.-I. Cho, C. R. D. Brown, T. Burian, J. Chalupský, K. Engelhorn, R. W. Falcone, C. Graves *et al.*, Phys. Rev. Lett. **109**, 065002 (2012).

[4] D. J. Hoarty, P. Allan, S. F. James, C. R. D. Brown, L. M. R. Hobbs, M. P. Hill, J. W. O. Harris, J. Morton, M. G. Brookes, R. Shepherd, J. Dunn, H. Chen, E. Von Marley, P. Beiersdorfer, H. K. Chung, R. W. Lee, G. Brown, and J. Emig, Phys. Rev. Lett. **110**, 265003 (2013).

[5] H. R. Griem, J. Phys. (Paris) Colloq. **49**, C1-293 (1988).

[6] R. Shepherd, P. Audebert, H.-K. Chen, K. Fournier, O. Peyreusse, S. Moon, R. Lee, D. Price, L. Klein, J. Gauthier, and P. Springer, J. Quant. Spectrosc. Radiat. Transfer **81**, 431 (2003).

[7] Y. Leng, J. Goldhar, H. R. Griem, and R. W. Lee, Phys. Rev. E **52**, 4328 (1995).

[8] O. Renner, D. Salzmann, P. Sondhauß, A. Djaoui, E. Krouský, and E. Förster, J. Phys. B **31**, 1379 (1998).

[9] A. Saemann, K. Eidmann, I. E. Golovkin, R. C. Mancini, E. Andersson, E. Förster, and K. Witte, Phys. Rev. Lett. **82**, 4843 (1999).

[10] U. Andiel, K. Eidmann, P. Hakel, R. C. Mancini, G. C. Junkel-Vives, J. Abdallah, and K. Witte, Europhys. Lett. **60**, 861 (2002).

[11] O. Renner, P. Adámek, P. Angelo, E. Dalimier, E. Förster, E. Krousky, F. B. Rosmej, and R. Schott, J. Quant. Spectrosc. Radiat. Transfer **99**, 523 (2006).

[12] C. R. Stillman, P. M. Nilson, S. T. Ivancic, I. E. Golovkin, C. Mileham, I. A. Begishev, and D. H. Froula, Phys. Rev. E **95**, 063204 (2017).

[13] N. Woolsey, J. Quant. Spectrosc. Radiat. Transfer **65**, 573 (2000).

[14] S. B. Hansen, E. C. Harding, P. F. Knapp, M. R. Gomez, T. Nagayama, and J. E. Bailey, High Energy Density Phys. **24**, 39 (2017).

[15] N. Hopps, K. Oades, J. Andrew, C. Brown, G. Cooper, C. Danson, S. Daykin, S. Duffield, R. Edwards, D. Egan *et al.*, Plasma Phys. Controlled Fusion **57**, 064002 (2015).

[16] D. Hillier, C. Danson, S. Duffield, D. Egan, S. Elsmere, M. Girling, E. Harvey, N. Hopps, M. Norman, S. Parker, P. Treadwell, D. Winter, and T. Bett, Appl. Opt. **52**, 4258 (2013).

[17] D. Riley, L. A. Gizzi, F. Y. Khattak, A. J. Mackinnon, S. M. Viana, and O. Willi, Phys. Rev. Lett. **69**, 3739 (1992).

[18] D. Riley and O. Willi, Phys. Rev. Lett. **75**, 4039 (1995).

[19] C. R. D. Brown, D. J. Hoarty, S. F. James, D. Swatton, S. J. Hughes, J. W. Morton, T. M. Guymer, M. P. Hill, D. A. Chapman, J. E. Andrew, A. J. Comley, R. Shepherd, J. Dunn, H. Chen, M. Schneider, G. Brown, P. Beiersdorfer, and J. Emig, Phys. Rev. Lett. **106**, 185003 (2011).

[20] D. J. Hoarty, S. F. James, C. R. D. Brown, B. M. Williams, H. K. Chung, J. W. O. Harris, L. Upcraft, B. J. B. Crowley, C. C. Smith, and R. W. Lee, High Energy Density Phys. **6**, 105 (2010).

[21] D. J. Hoarty, P. Allan, S. F. James, C. R. D. Brown, L. M. R. Hobbs, M. P. Hill, J. W. O. Harris, J. Morton, M. G. Brookes, R. Shepherd, J. Dunn, H. Chen, E. Von Marley, P. Beiersdorfer, H. K. Chung, R. W. Lee, G. Brown, and J. Emig, High Energy Density Phys. **9**, 661 (2013).

[22] P. Beiersdorfer, E. W. Magee, G. V. Brown, H. Chen, J. Emig, N. Hell, M. Bitter, K. W. Hill, P. Allan, C. R. D. Brown, M. P. Hill, D. J. Hoarty, L. M. R. Hobbs, and S. F. James, Rev. Sci. Instrum. **87**, 063501 (2016).

[23] P. Beiersdorfer, J. Clementson, J. Dunn, M. F. Gu, K. Morris, Y. Podpaly, E. Wang, M. Bitter, R. Feder, K. W. Hill, D. Johnson, and R. Barnsley, J. Phys. B **43**, 144008 (2010).

[24] P. Beiersdorfer, E. W. Magee, N. Hell, and G. V. Brown, Rev. Sci. Instrum. **87**, 11E339 (2016).

[25] N. Hell, P. Beiersdorfer, E. W. Magee, and G. V. Brown, Rev. Sci. Instrum. **87**, 11D604 (2016).

[26] P. Beiersdorfer, E. W. Magee, G. V. Brown, N. Hell, A. McKelvey, R. Shepherd, D. J. Hoarty, C. R. D. Brown, M. P. Hill, L. M. R. Hobbs, S. F. James, and L. Wilson, Rev. Sci. Instrum. **89**, 10F120 (2018).

[27] P. Beiersdorfer, G. V. Brown, R. Shepherd, P. Allan, C. R. D. Brown, M. P. Hill, D. J. Hoarty, L. M. R. Hobbs, S. F. James, H. K. Chung, and E. Hill, Phys. Plasmas **23**, 101211 (2016).

[28] X. Li and F. B. Rosmej, Europhys. Lett. **99**, 33001 (2012).